2.5-D Multi-Phase Topology Optimization of Permanent Magnet Motor Using Gaussian Basis Function

Yoshitsugu Otomo[1,2], Hajime Igarashi[1], Tomohiro Sato[3], Yoshihisa Suetsugu[3], and Eiji Fujioka[3]

[1]Graduate School of Information Science and Technology, Hokkaido University, Sapporo 060-0814, Japan
[2]Research Fellow of Japan Society for the Promotion of Science (JSPS), Tokyo 102-0083, Japan
[3]AISIN Corporation, Kariya 448-8650, Japan

This paper proposes a novel 2.5-D multi-phase topology optimization method using a Gaussian basis function for permanent magnet motors. The design region in the rotor was sliced into cylindrical layers; two-dimensional topology optimization was performed for each layer such that the average torque was maximized while the torque ripple was suppressed to the maximum possible extent. The proposed topology optimization could determine the rotor core and magnet shapes, as well as the magnetization direction. It was shown that the optimized 2.5-D topology optimization led to better torque performance when compared to conventional 2-D optimizations.

***Index Terms*—Magnetization, Multi-phase topology optimization, NGnet, Permanent magnet motor.**

I. Introduction

HIGH PERFORMANCE permanent magnet (PM) motors are required for electric vehicles and plug-in hybrid vehicles to realize low electricity consumption and high torque density. To improve the performance of PM motors, the PM and flux-barrier shapes and magnetization directions have been expressed by a set of parameters for optimal design [1, 2]. Although this approach can improve motor performance, it does not lead to the development of novel structures that deliver outstanding performance.

In contrast to the above-mentioned parameter-based optimization, the topology optimization in which the material shape is freely deformed allowing the generation and annihilation of holes can lead, in principle, to novel machine structures [3]–[7]. Topology optimization that represents material distribution using Gaussian basis functions is effective for the design of rotating machines [5]–[7]. This method can deal with multi-phase topology optimization, which simultaneously determines the distributions of flux barriers, magnetic materials, and permanent magnets with different magnetizations. However, when this method was applied to 3-D motor models, by which the leakage flux at the rotor end was taken into consideration, the performance of the optimized motor was not consistently superior to that of 2-D models. This was owing to the fact that the degrees of freedom (DoFs) of the 3-D multi-phase topology optimization were excessively large and hindered the process to obtain an optimal machine structure. Thus, it was necessary to reduce DoFs without losing the merit of 3-D optimization.

In this paper, we propose a 2.5-D multi-phase topology optimization method for PM motors. In the proposed method, a 3-D motor model was sliced into cylindrical layers and 2-D topology optimization was applied to each layer. The entire motor property was improved by simultaneously performing 2-D optimizations. In the proposed optimization, we optimized the rotor shape of the PM motor such that the average torque was maximized while the torque ripple was suppressed to the maximum possible extent.

Manuscript received January 24, 2022; revised April 25, 2022; accepted April 27, 2022. Corresponding author: Y. Otomo.

Color versions of one or more of the figures in this paper are available online at http://ieeexplore.ieee.org.

Digital Object Identifier (inserted by IEEE).

II. Optimization Method

For a 2-D multi-phase topology optimization using Gaussian basis functions [6, 7], we introduce the shape functions $y_1(\boldsymbol{x}, \boldsymbol{w}^1)$ and $y_2(\boldsymbol{x}, \boldsymbol{w}^2)$ defined by

$$y_k(\boldsymbol{x}, \boldsymbol{w}^k) = \sum_{i=1}^{N} w_i^k b_i(\boldsymbol{x}), \quad (k = 1, 2), \tag{1}$$

where $w_i^k \in [-1, 1]$, $\boldsymbol{x}$, and N denote the weighting coefficient for the k-th shape function y_k, position vector, and number of Gaussian functions, respectively. Moreover, $b_i(\boldsymbol{x})$ is a normalized Gaussian function, given by

$$b_i(\boldsymbol{x}) = G_i(\boldsymbol{x}) \Big/ \sum_{j=1}^{N} G_j(\boldsymbol{x}), \tag{2}$$

$$G_i = \frac{1}{2\pi\sigma^2} \exp\left\{-\frac{1}{2\sigma^2}|\boldsymbol{x} - \boldsymbol{x}_i|^2\right\}, \tag{3}$$

where σ and $\boldsymbol{x}_i$ denote the standard deviation and center of the Gaussian basis, respectively. The material type (attribute) M_e of finite element e in the design region Ω_{core} is determined from the angle $\theta = \tan^{-1}\{y_2(\boldsymbol{x}, \boldsymbol{w}^2)/y_1(\boldsymbol{x}, \boldsymbol{w}^1)\}$ defined in the state space shown in Fig. 1 as follows:

$$M_e = \begin{cases} \text{Air}, & 0 \le \theta < 150 \\ \text{Iron}, & 150 \le \theta < 300 \\ \text{Magnet}, & 300 \le \theta < 360 \end{cases} \tag{4}$$

In the proposed 2-D optimization, $\boldsymbol{w}^1$, $\boldsymbol{w}^2$, and the magnetization direction θ_{m} of the permanent magnet in Ω_{core} were determined in order to minimize the objective function using the covariance matrix adaptation evolution strategy (CMA-ES) [8], whose performance was experientially found to be better in general than the generic algorithm (GA). CMA-ES

generates the population according to the Gaussian distribution so that it expands and contracts as it approaches the optimal solution.

The reference PM motor and optimization model are shown in Figs. 2 and 3, where the green arrows on the permanent magnets represent the magnetization. Table I summarizes the model parameters and driving conditions. The optimization model was sliced into three layers along the rotating shaft for the proposed 2.5-D optimization, although the number of layers may be arbitrary. The structure of each layer was determined such that the torque characteristics of the entire motor model were optimized. In the proposed optimization, $\boldsymbol{p} = [\boldsymbol{w}^{1-\text{Layer }1}, \boldsymbol{w}^{2-\text{Layer }1}, \dots, \boldsymbol{w}^{1-\text{Layer }L}, \boldsymbol{w}^{2-\text{Layer }L}, \theta_{\text{m}}]^{\text{t}} \in \mathbb{R}^{2NL+1}$ contained the optimization variables determined by CMA-ES, where $\boldsymbol{w}^{k-\text{Layer }l}$ and L denote the weighting coefficients in (1) for the l-th layer and the number of layers, respectively. The schematic of the above-mentioned 2.5-D topology optimization is shown in Fig. 4.

III. Optimization of PM Motor

A. Optimization Problem

The purpose of the optimization was to maximize the average torque while minimizing the torque ripple. Thus, we solved the optimization problem defined by

$$\min_{\boldsymbol{p}} F(\boldsymbol{p}), \quad F(\boldsymbol{p}) = -\frac{T_{\text{avg}}(\boldsymbol{p})}{T_{\text{avg}}^{\text{Ref}}} + 0.05\frac{T_{\text{rip}}(\boldsymbol{p})}{T_{\text{rip}}^{\text{Ref}}}, \quad \text{sub. to } V_{\text{mag}}(\boldsymbol{p}) \le V_{\text{mag}}^{\text{Ref}}, \tag{5}$$

where $T_{\text{avg}}(\boldsymbol{p}) = \frac{1}{n}\sum_{i=1}^{n} T_i(\boldsymbol{p})$, $T_{\text{rip}}(\boldsymbol{p}) = \left\{\max_i T_i(\boldsymbol{p}) - \min_i T_i(\boldsymbol{p})\right\}/T_{\text{avg}}(\boldsymbol{p})$, $T_i(\boldsymbol{p})$, n, and $V_{\text{mag}}(\boldsymbol{p})$ denote the average torque, torque ripple, i-th instantaneous torque, number of analysis steps, and magnet volume, respectively, and the quantities for the reference motor are marked with superscript "Ref". It is noted that the overall torque $T_i(\boldsymbol{p})$ for the rotor composed of all the layers was computed using the nodal force method [9]. We imposed the volume constraint in (5) using the oracle penalty method [10].

B. Optimization Setting

To validate the performance of the proposed 2.5-D topology optimization, we further solved (5) using 2-D topology optimization [6, 7]. The solution for the latter case was obtained by simply setting $L = 1$ in the proposed 2.5-D optimization. The distribution of the Gaussian basis functions for the 2-D and 2.5-D topology optimizations is shown in Fig. 5. The quarter design region was covered by circles representing the region of influence of the Gaussian basis functions centered at $\boldsymbol{x}_i$. We assumed mirror symmetry of the rotor structure. In addition, the definitions of the magnetization directions $\theta_{\text{m}} \in [90, 180]$ in the design region are shown in Fig. 6. Although we could consider the magnetization direction parallel to the rotating shaft, only the radial magnetization was considered for the sake of simplicity.

In this optimization, according to the recommendations of

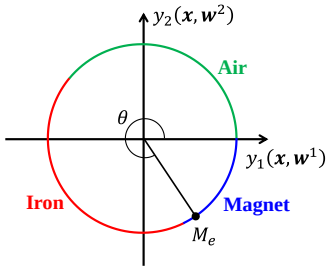

Fig. 1. State space for multi-phase optimization

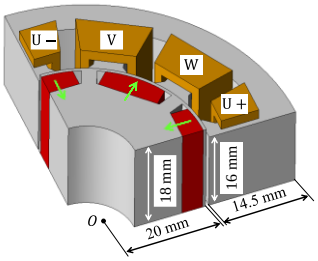

Fig. 2. Reference model (1/8 fraction is shown.)

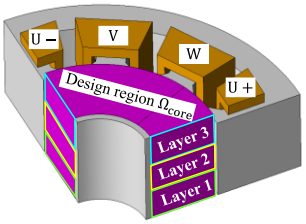

Fig. 3. Optimization model

TABLE I
Specifications of Reference PM Motor

Phase and pole	Three-phase, eight poles
Coil current (A)	15
Driving frequency (Hz)	200 / 3
Initial electric angle (deg)	15
Initial mechanical angle (deg)	0
Number of coil turns	25
Rotating speed (r/min)	1000
Magnetization of magnet (T)	1.2
Rotor and stator grade	50A270

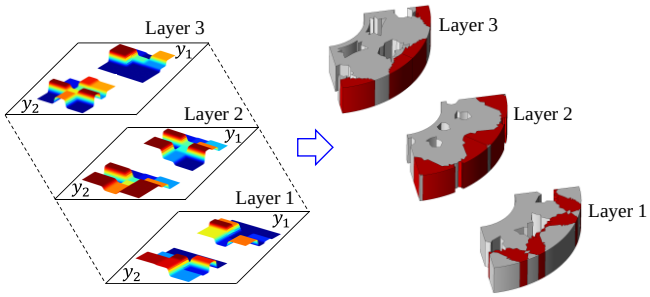

Output of shape functions in Ω_{core} — Resultant rotor shapes

Fig. 4. Schematic of proposed 2.5-D optimization

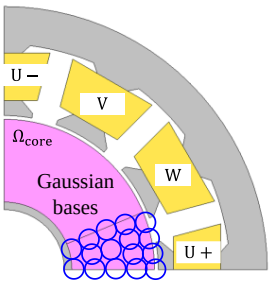

Fig. 5. Distribution of Gaussian basis functions ($N = 16$, $\sigma = 1.3$ mm)

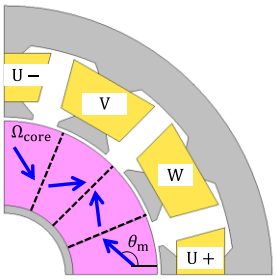

Fig. 6. Magnetization direction θ_{m}

CMA-ES, $5 \times \{4 + \lfloor 3\ln(2NL+1)\rfloor\}$ individuals were generated for the first iteration, and these were updated by the $(\mu/\mu_{\text{W}}, \lambda)$-CMA-ES at each iteration [8]. The optimization

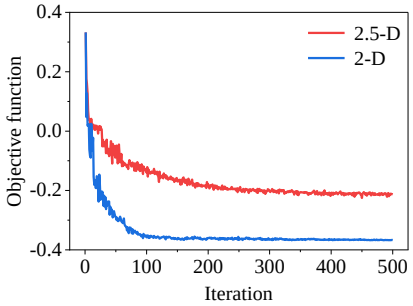

Fig. 7. Convergence histories of 2-D and 2.5-D optimizations

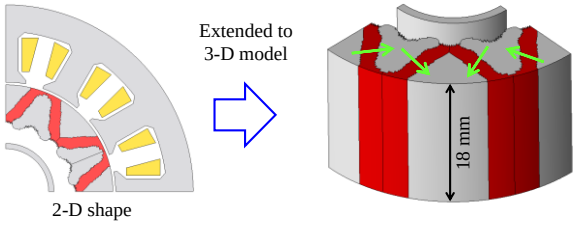

Fig. 8. Resultant rotor shape obtained by 2-D topology optimization ($V_{\mathrm{mag}} = 0.97V_{\mathrm{mag}}^{\mathrm{Ref}}$, $\theta_{\mathrm{m}} = 140$ deg)

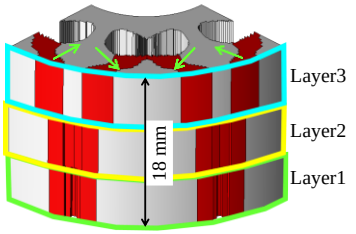

(a) Bird view

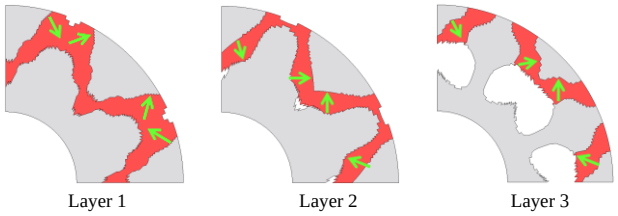

(b) Cross sectional view of each layer

Fig. 9. Resultant rotor shape obtained by 2.5-D topology optimization ($V_{\mathrm{mag}} = 0.98V_{\mathrm{mag}}^{\mathrm{Ref}}$, $\theta_{\mathrm{m}} = 137$ deg)

process was continued for more than 500 iterations. It took approximately 1.8 h and three days for the 2-D and 2.5-D optimizations, respectively, to obtain the optimization results using the Intel Xeon CPU (3.5 GHz, 32 threads).

IV. Optimization Results

A. 2-D and 2.5-D Optimizations

The convergence histories of the 2-D and 2.5-D optimizations are plotted in Fig. 7. The value of $F(\boldsymbol{p})$ for the 2-D optimization becomes constant after approximately 100 iterations, whereas that for the 2.5-D optimization continues to reduce over approximately 250 iterations. This is because the DoFs of the 2.5-D optimization are three times larger than those of the 2-D optimization. The final value of $F(\boldsymbol{p})$ for the 2-D model was smaller than that of the 2.5-D model because the former neglected the end effect. In fact, $F(\boldsymbol{p})$ became larger for

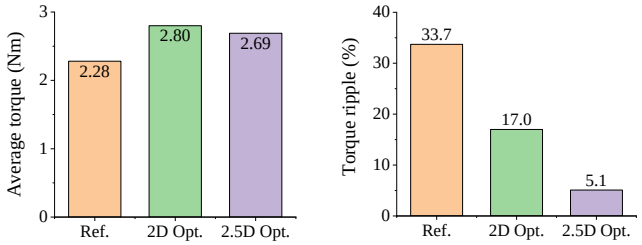

(a) Average torque (b) Torque ripple

Fig. 10. Average torque and torque ripple

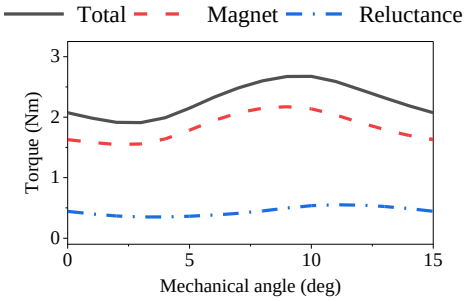

(a) Reference

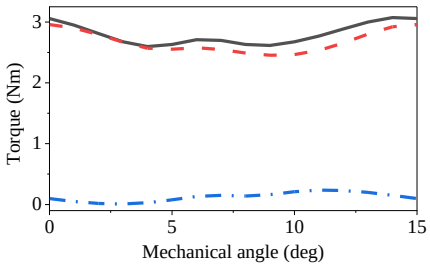

(b) 2-D optimization

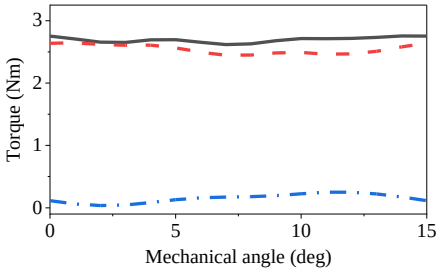

(c) 2.5-D optimization

Fig. 11. Torque waves for reference and resultant shapes

the 3-D model whose rotor was obtained by extruding the rotor of the 2-D model, as will be mentioned below.

The resultant rotor shapes obtained by 2-D and 2.5-D optimizations are shown in Figs. 8 and 9, where the magnet volume and magnetization direction are shown in the caption. We can see that the rotor shape obtained by the 2-D optimization had V-shaped magnets such that the magnetic flux was concentrated along the d-axis. The rotor obtained by the 2.5-D optimization also had V-shaped magnets with different depths for each layer. It should be noted that we had various rotor structures that differed for each layer, for example, the rotor structures of a surface magnet motor and reluctance motor when we changed the optimization settings.

The average torque and torque ripple for the reference and optimized shapes are shown in Fig. 10. Note that the torque characteristics for the PM motor obtained via 2-D optimization

were computed using a 3-D model shown in Fig. 8. We can see that the average torque values for the resultant rotor shapes in Figs. 8 and 9 were approximately 20 % larger than that of the reference model, although the magnet volume remained almost unchanged. The proposed method considerably improved the torque ripple compared to the reference model while the 2-D optimization method improved it moderately. To understand the difference in the performance among these rotor shapes, we compared the torque waves shown in Fig. 11, in which the total torque was decomposed into magnet and reluctance torques by the frozen permeability method [11]. It could be seen that the optimized shapes had larger magnet torques than the reference model. The ripple in the magnet torque in Fig. 11 (b) was approximately 10 % larger than that in Fig. 11 (c). This was one of the reasons why the rotor in Fig. 9 had a smaller torque ripple than that in Fig. 8. Moreover, to compare the torque performances of the optimized shapes in detail, the torque waves in the three layers were computed using the nodal force method [9]. The results are presented in Fig. 12. Note that the decomposed torques added up to the total torque, as shown in Fig. 11. We can see that the torque variations in layers 1 and 3 of the 2.5-D model were canceled out. In contrast, the torques of the 2-D model were in phase, such that the variations did not cancel out. It is well known that torque variations can be canceled out by skewed rotors as well. The 2.5-D structure shown here is *a new alternative* for the reduction of torque ripples.

B. *Smoothing of Rotor Shape for Manufacturing*

It may be difficult to manufacture the rotor shapes resulting from our proposed method because the core and magnet surfaces are wavy. To overcome this problem, we made the magnet surfaces smoother. A typical smoothing result is presented in Fig. 13. We can see that smoothing had little impact on the torque performance, as shown in Fig. 13 (c).

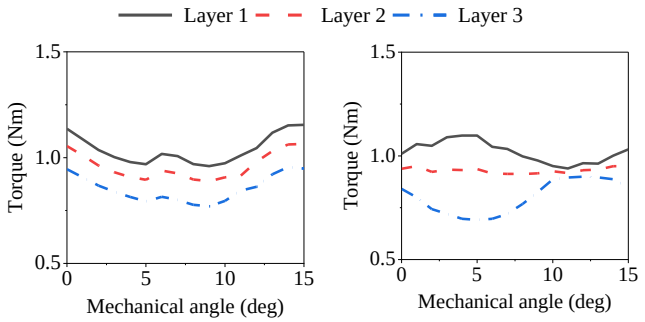

(a) 2-D optimization (b) 2.5-D optimization

Fig. 12. Decomposed torque waves for each layer

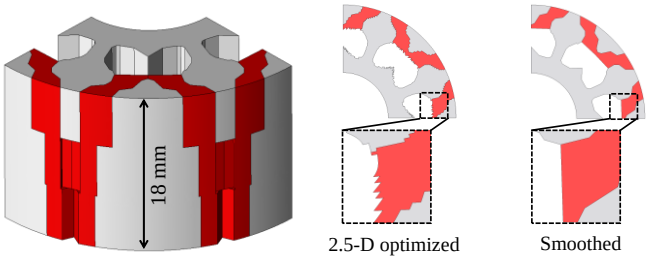

(a) Bird view of smoothed rotor (b) Cross sectional view of layer 3

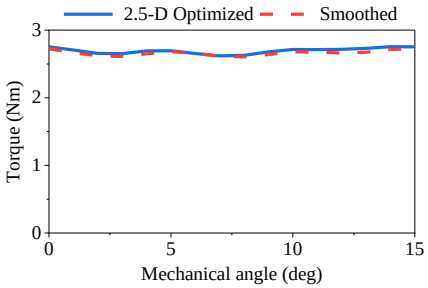

(c) Torque waves for 2.5-D optimized and smoothed shapes

Fig. 13. Smoothed rotor shape and torque waves

V. Conclusion

In this paper, we proposed a novel 2.5-D multi-phase topology optimization method for PM motors using a Gaussian basis function. It has been shown that the proposed method could significantly reduce torque ripples and simultaneously increase the average torque. The novel 2.5-D rotor structure obtained in this study is a new alternative to skewed rotors. In the future, we plan to manufacture an optimized rotor to verify its performance through experiments.

Acknowledgment

This work was supported in part by the JSPS KAKENHI under Grant JP19J20375 and Grant JP21H01301. The authors thank Editage for editing the draft of this article.

References

[1] Y. Yang, *et al.*, "Design and Comparison of Interior Permanent Magnet Motor Topologies for Traction Applications," *IEEE Trans. Transport. Electrific.*, vol. 3, no. 1, pp. 86-97, 2017.

[2] D. Lim, *et al.*, "Optimal Design of Interior Permanent Magnet Synchronous Motor by Using a New Surrogate-Assisted Multi-Objective Optimization," *IEEE Trans. Magn.*, vol. 51, no. 11, Art. no. 8207504, 2015.

[3] A. Khan, C. Midha, and D. A. Lowther, "Sequence-Based Environment for Topology Optimization," *IEEE Trans. Magn.*, vol. 56, no. 3, Art. no. 7510904, 2020.

[4] S. Barmada, N. Fontana, A. Formisano, D. Thomopulos, and M. Tucci, "A Deep Learning Surrogate Model for Topology Optimization," *IEEE Trans. Magn.*, vol. 57, no. 6, Art. no. 7200504, 2021.

[5] S. Hiruma, M. Ohtani, S. Soma, Y. Kubota, and H. Igarashi, "Novel Hybridization of Parameter and Topology Optimizations: Application to Permanent Magnet Motor," *IEEE Trans. Magn.*, vol. 57, no. 7, Art. no. 8204604, 2021.

[6] T. Sato, K. Watanabe, and H. Igarashi, "Multimaterial Topology Optimization of Electric Machines Based on Normalized Gaussian Network," *IEEE Trans. Magn.*, vol. 51, no. 3, Art. no. 7202604, 2015.

[7] H. Sato, S. Hiruma, and H. Igarashi, "Multi-material Topology Optimization of Permanent Magnet Motor with Arbitrary Adjacency Relationship of Materials," in *Proc. IEEE CEFC 2020*, DOI: 10.1109/CEFC46938.2020.9451380, pp. 1-4, 2020.

[8] N. Hansen, "The CMA Evolution Strategy: A Tutorial," arXiv:1604.00772, pp. 1-39, 2016.

[9] A. Kameari, "Local force calculation in 3D FEM with edge element," *IJAEM*, vol. 3, pp. 231-240, 1993.

[10] M. Schluter and M. Gerdts, "The oracle penalty method," *J. Global Optim.*, vol. 47, no. 2, pp. 293-325, 2010.

[11] W. Q. Chu and Z. Q. Zhu, "Average Torque Separation in Permanent Magnet Synchronous Machines Using Frozen Permeability," *IEEE Trans. Magn.*, vol. 49, no. 3, pp. 1202-1210, 2013.